Intrinsic Strength and Failure Behaviors of Graphene Grain Boundaries

Junfeng Zhang,[†] Jijun Zhao,[†,*] and Jianping Lu[‡,*]

[†]Key Laboratory of Materials Modification by Laser, Ion and Electron Beams, Dalian University of Technology, Ministry of Education, Dalian 116024, People's Republic of China, and [‡]Department of Physics and Astronomy, University of North Carolina at Chapel Hill, Chapel Hill, North Carolina 27599, United States

ABSTRACT

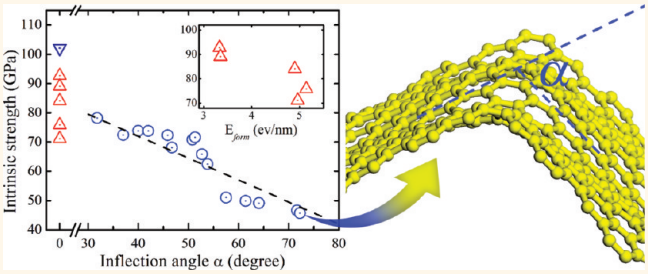

As one-dimension line defects, grain boundaries (GBs) can affect many intrinsic properties of graphene. In this paper, the mechanical properties of 20 representative graphene grain boundaries were studied using density functional theory and molecular dynamics. With different arrangements of the pentagonal and heptagonal rings, the grain boundary may remain flat or become inflected up to 72°. For the flat GBs, the intrinsic tensile strength decreases linearly with the formation energy with a maximum value of 93 GPa, close to that of a perfect graphene. The intrinsic tensile strength of the inflected GBs is found to generally decrease with increasing inflection angle. Stone–Wales transformation is identified as the major failure mechanism of graphene GBs at high temperatures, whereas the initial fracture site can be either on the boundary line or inside the domain. These theoretical results constitute a useful picture of the grain boundary effect on the mechanical properties of polycrystalline graphene.

KEYWORDS: graphene · grain boundary · defects · tensile strain · intrinsic strength

With its extraordinary mechanical and electronic properties, graphene holds great promise for a variety of applications.[1,2] Stiffness and strength are the key factors in determining the stability and lifetime of many devices. As one of the strongest materials, pristine graphene possesses an ultrahigh Young's modulus of ~1 TPa and an intrinsic fracture strength of ~130 GPa.[3] However, in realistic graphene materials there are always some structural defects.[1,4−6] It was found that isolated defects, such as monovacancies and Stone−Wales dislocations,[7] slits,[8,9] and holes,[9] would affect the mechanical properties of graphene. For instance, Young's modulus of a monolayer graphene sheet decreases slowly with vacancy concentration,[8] while inclusion of large slits or holes reduces drastically the fracture strength of graphene sheets to 30−40 GPa.[8,9]

In addition to the isolated defects, extended one-dimensional (1D) defects such as grain boundaries (GBs) are frequently observed in graphene.[6,10−16] Especially, in the experimental fabrication of large-scale graphene using the chemical vapor deposition (CVD) method, obtaining a polycrystalline flake composed of many single-crystal domains separated by GBs is almost inevitable. The existence of GBs would affect the mechanical and electronic properties of graphene and consequently have significant impact on their device applications.

Recently, the structures, stability, and electronic properties of graphene GBs have been intensively studied,[11−22] but less is known about their mechanical properties. AFM measurement of polycrystalline graphene by Huang *et al.* demonstrated that GBs can severely weaken the mechanical strength of graphene membranes; namely, the fracture load decreased by an order of magnitude.[14] For selected symmetric GBs, Grantab *et al.*[23] simulated the ultimate strengths and found that a graphene sheet with large misorientation angles and high densities of defects can be nearly as strong as pristine graphene, while the failure strength is much smaller for some GBs with small misorientation angles. However, little is known about the mechanical properties of more general (nonsymmetric graphene) GBs. In this work, we systematically explored the intrinsic strengths and failure behaviors of 20 representative graphene GBs (both symmetric and nonsymmetric) under tensile strains. We found that the intrinsic

* Address correspondence to zhaojj@dlut.edu.cn (J.J.Z.), jpl@physics.unc.edu (J.P.L.).

Received for review January 11, 2012 and accepted February 27, 2012.

Published online February 27, 2012
10.1021/nn3001356

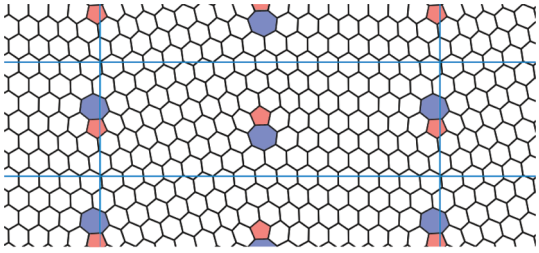

(a) (4, 2)|(3, 3) (Topview)

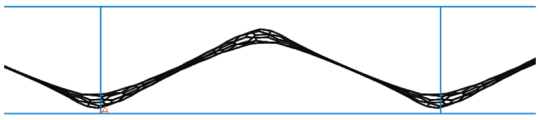

(b) (4, 2)|(3, 3) (Sideview)

Figure 1. Example of supercell used for our calculation. Shown is the GB (4, 2)|(3, 3) structure with supercell parameter of 3.812 × 1.279 × 1.2 nm from (a) top view and (b) side view.

strength of a graphene GB depends mainly on its inflection angle rather than other geometry parameters. We also found that the fracture failure of a graphene GB can initiate from either the grain boundary or inside the domain, depending on the defect arrangement as well as the lattice orientation of the graphene domains.

RESULTS AND DISCUSSION

Structures and Formation Energy. A graphene GB can be described by the two periodic translation vectors (n_L, m_L) and (n_R, m_R) of left and right domains along the defect line as (n_L, m_L)|(n_R, m_R).[18] For an infinite GB with periodically arranged defects, the period along the GB for the two domains are given by $L_L = |n_L\vec{a}_1 + m_L\vec{a}_2| = a_0(n_L^2 + n_L m_L + m_L^2)^{1/2}$ and $L_R = |n_R\vec{a}_1 + m_R\vec{a}_2| = a_0(n_R^2 + n_R m_R + m_R^2)^{1/2}$, respectively, where $a_0 = |\vec{a}_1| = |\vec{a}_2| = 0.246$ nm is the unit vector length of the graphene lattice. The misorientation angle between the two domains is given by $\theta = \tan^{-1}[\sqrt{3}m_L/(m_L + 2n_L)] + \tan^{-1}[\sqrt{3}m_R/(m_R + 2n_R)]$.

In principle, there are many possibilities for the periodic lengths and the defect arrangements along a boundary line. However, to form a physically realistic GB, its formation energy has to be reasonably low. Indeed, the formation energy of a GB originates from two contributions: the mismatch energy due to the difference between the periodic lengths of the two domains and the defect energy due to the inclusion of nonhexagonal rings. For symmetric GBs the lattice mismatch part is zero as $L_L = L_R$. For a nonsymmetric GB with $L_L \neq L_R$, too large a mismatch between L_L and L_R results in very high formation energy. To achieve stable GBs with small deformations and reasonable formation energies, here we filtered GBs with a threshold mismatch of 5% (with a maximum formation energy of 5.6 eV/nm) and considered 20 combinations of (n_L, m_L) and (n_R, m_R) up to a periodic length of 1.7 nm along the grain boundary direction. Along the GB line defect rings of quadrilaterals, octagons, or nonagons were ruled out since they are usually thermodynamically unstable and are seldom observed in experiments.[12,14] It is noteworthy that some complex and large-scale distortions (like wrapping and scrolling)[24] could be induced due to lattice mismatch in a realistic graphene sample with a grain boundary; however these defect are nonperiodic along the defects line, thus beyond the scope of our investigation.

All 20 GBs explored here are shown in Figure 2. According to the arrangement of pentagons and heptagons, these GBs can be categorized into four classes: (I) pentagon−heptagon pairs periodically separated by one or more hexagons, (II) two or more adjacent pentagon−heptagon pairs separated by one or more hexagons, (III) isolated pentagons or heptagons on the boundary with or without pentagon−heptagon pairs, (IV) periodically repeated pentagon−heptagon pairs constituting an entire boundary. Isomers with the same misorientation angle or translation vector (n_L, m_L)|(n_R, m_R) but with different arrangement of the defect rings are labeled (n_L, m_L)|(n_R, m_R)-iN (N = 1, 2, ...), as shown in Figure 2.

Thermodynamic stability of a GB can be measured in terms of the formation energy per unit length (E_{form}) calculated by

$$E_{form} = (E_{GB} - N \times E_{graphene})/2L \quad (1)$$

where E_{GB} stands for the energy of the entire GB supercell, $E_{graphene}$ is the energy per carbon atom for the pristine graphene, N is the number of carbon atom in the supercell, L is the periodic length along the GB, and the factor 2 accounts for two GBs in one supercell. All of the theoretical data (inflection angles, misorientation angles, periodic lengths, formation energies, critical failure strains, and intrinsic strengths) of the 20 GBs explored are summarized in Table 2. The formation energies and periodic lengths agree well with previous theoretical results from DFT,[18,19] DFTB,[20] and empirical molecular dynamics (MD)[21] calculations. The formation energy for GBs ranges between 2.5 and 6.0 eV/nm, lower than that of the bare graphene edges (~10 eV/nm).[25] GBs with the same misorientation angle but different defect configurations are found to have similar formation energy and thus have similar probability during the formation process. For example, the difference in formation energy between (4, 1)|(4, 1)-i1 and (4, 1)|(4, 1)-i2 is ΔE = 0.6 eV/nm, and the difference between (5, 2)|(6, 1)-i1 and (5, 2)|(6, 1)-i2 is 0.33 eV/nm. This suggests that the formation energy is dominated by the lattice mismatch, not the defect configuration. This explains why some GBs with high defect density (*e.g.*, the (3, 1)|(3, 1)-i2 GB in Figure 2) do not necessarily possess high formation energy if the defect rings are appropriately arranged to accommodate the tension energy.

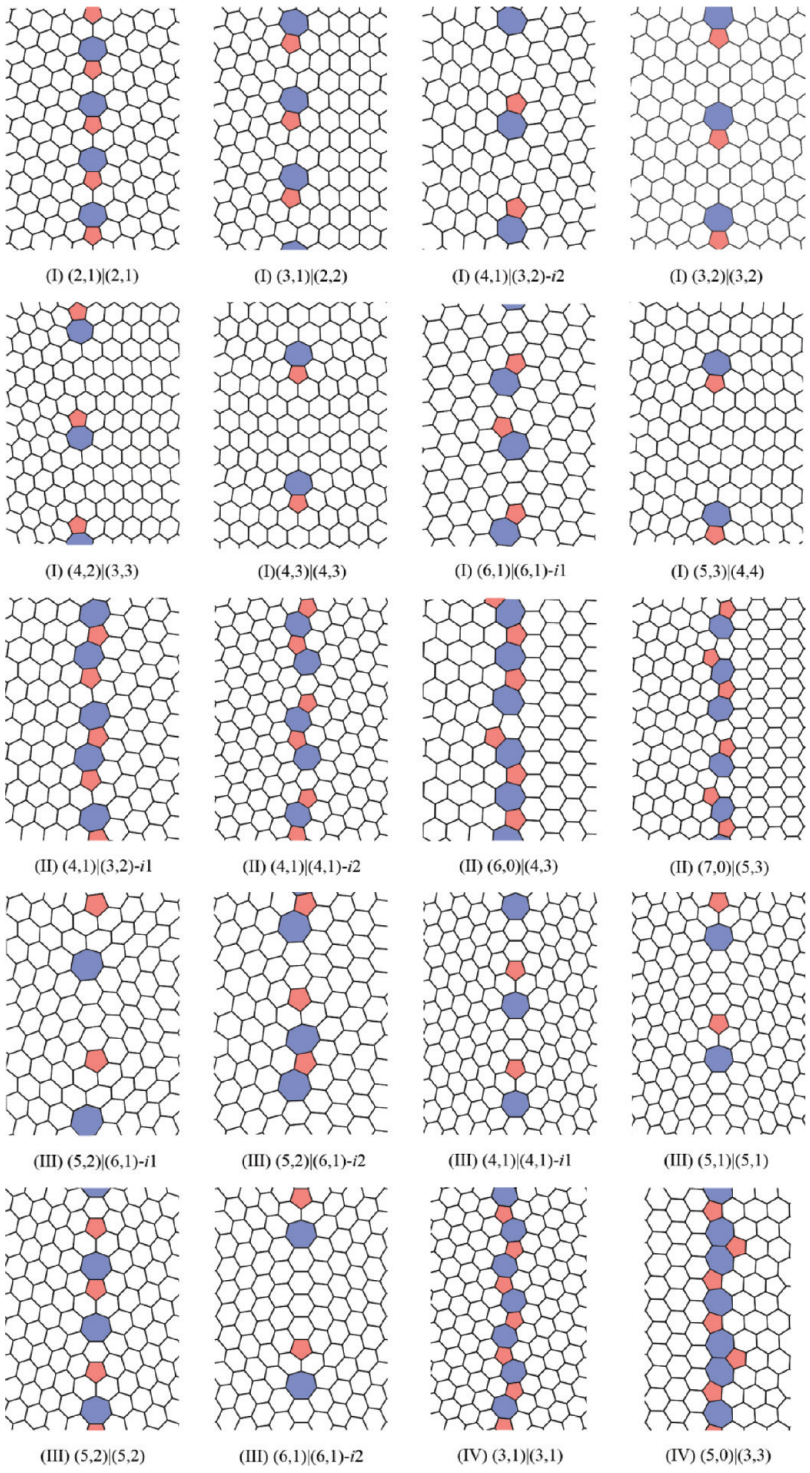

Figure 2. Structures for the 20 GBs considered in this work. Depending on arrangements of the defects rings, the 20 GBs are classified into four classes (I−IV).

A GB can either be flat like pristine graphene or cause an inflection angle α between the two domains,[20] as shown in Table 2. Our results demonstrate that there is no clear correlation between the inflection angle and the mismatch strain along the boundary, and the inflection is mainly determined by the arrangement of defects on the boundary. Figure 3 shows the formation energies and the intrinsic strengths of the 20 GBs as functions of either inflection angle α or misorientation angle θ, respectively. As shown in Figure 3a, the formation energies of graphene GBs show no clear dependence on α. Some highly inflected GBs such as (5, 3)|(4, 4) or (4, 3)|(4, 3) can be as stable as the flat ones. The average bond

TABLE 1. Calculated Inflection Angles (α), Intrinsic Strengths (τ), and Critical Failure Strains (δ) for Selected GBs with Different Periodic Spacing *d* between the GBs[a]

GB	*d* (nm)	α (deg)	τ (GPa)	δ (%)
(4, 1)|(3, 2)-*i*1	1.188	31.8	78	14
	1.417	31.5	79	15
	1.698	31.3	79	14
	1.926	31.3	79	14
(4, 2)|(3, 3)	1.238	50.8	71	19
	1.460	50.2	70	19
	1.683	50.2	68	19
	1.906	50.3	68	19
(4, 1)|(4, 1)-*i*1	1.328	71.8	47	24
	1.521	71.0	46	24
	1.713	70.0	48	25
	1.906	70.0	47	25

[a] Beyond 2 nm spacing, the calculate GB properties are independent of *d* (the supercell size is 2*d* along the *y* axis..

length (1.496 Å) of a heptagon and the bond angle (109.32°) of a pentagon found in the (5, 3)|(4, 4) GB suggest local sp^3 hybridization. Similar results are found for the (4, 3)|(4, 3) GB (bond length 1.497 Å and bond angle 109.61°). Such local sp^3 hybridization associated with buckled GBs may compensate the tension due to pentagon or heptagon rings and may be responsible for the high chemical reactivity of the boundary.[16,20] The dependence of the lowest E_{form} on the misorientation angle θ conforms roughly with the previously proposed sin(3θ) function,[17] as shown in Figure 3c.

Intrinsic Strengths. From our DFT calculations, the intrinsic strength (defined as the stress point beyond which the stress decreases with strain) of a GB shows no clear correlation with the misorientation angle θ (Figure 3d), but exhibits interesting dependence on the inflection angle α (Figure 3b). Generally speaking, the buckled GBs possess lower strength (46−78 GPa) with regard to the flat ones (71−93 GPa). As shown by the dashed line of Figure 3b, the intrinsic strength (τ) of those inflected GBs can be fitted into a linear function empirically:

$$\tau\ (\text{inGPa}) = \tau_0 - 0.75\alpha\ (\text{indeg}) \qquad (2)$$

where τ_0 = 102 GPa is the calculated intrinsic strength of graphene in the zigzag direction. In other words, inflection of the grain boundary significantly decreases the mechanical strength of a graphene flake.

For the flat GBs (α = 0°), an intrinsic strength as high as 93 GPa can be achieved (see Figure 4). This is almost comparable to that of perfect graphene (102 or 113 GPa). A recent DFT study by Grantab *et al.*[23] predicted an intrinsic strength of ∼95 GPa for the flat symmetric (2, 1)|(2, 1) and (3, 1)|(3, 1) GBs, in agreement with the present results. Moreover, as shown in the inset graph of Figure 3b, the strength of flat GBs correlates well with the formation energy; that is, a

TABLE 2. Structural, Energetic, and Mechanical Properties of the 20 GBs Calculated[a]

GB	α (deg)	θ (deg)	*L* (nm)	E_{form} (eV/nm)	δ (%)	class	τ (GPa)
graphene(ZZ)	0	0	0.246	0	19		102
graphene(AC)	0	0	0.246	0	23		113
(3, 1)|(3, 1)	0	32.2	0.889	3.3	11	IV	93
					2.8[19]		∼95[23]
(2, 1)|(2, 1)	0	21.8	0.654	3.4	14	I	89
			0.65[19]	3.4,[19] 4.0,[17] 4.3[21]			∼93[23]
(6, 0)|(4, 3)	0	34.7	1.481	4.9	12	II	84
(5, 0)|(3, 3)	0	30.0	1.239	5.1	10	IV	76
			1.250[19]	5.0[19]			
(6, 1)|(6, 1)-*i*1	0	44.8	1.622	5.0	12	I	71
(4, 1)|(3, 2)-*i*1	31.80	31.8	1.095	5.6	14	II	78
(4, 1)|(4, 1)-*i*2	37.00	38.2	1.127	4.1	15	II	72
							∼57[23]
(7, 0)|(5, 3)	40.00	38.2	1.709	4.8	13	II	74
(3, 1)|(2, 2)	42.00	16.1	0.868	5.1	16	I	74
(3, 2)|(3, 2)	45.85	13.2	1.065	3.6	19	I	72
(5, 3)|(4, 4)	46.70	8.2	1.690	2.8	13	I	68
(4, 2)|(3, 3)	50.80	10.9	1.279	3.4	16	I	71
(4, 3)|(4, 3)	51.30	9.4	1.483	3.0	18	I	72
(5, 2)|(6, 1)-*i*2	52.70	36.3	1.540	4.8	17	II	66
(4, 1)|(3, 2)-*i*2	53.80	25.7	1.111	4.7	21	I	63
(5, 2)|(5, 2)	57.50	27.8	1.529	4.7	19	III	51
(6, 1)|(6, 1)-*i*2	61.40	44.8	1.578	3.8	20	III	50
(5, 2)|(6, 1)-*i*1	64.04	36.3	1.506	5.1	17	III	49
(4, 1)|(4, 1)-*i*1	71.67	38.2	1.117	4.7	24	III	47
(5, 1)|(5, 1)	72.22	42.1	1.355	4.4	23	III	46
							∼49[23]

[a] α is for inflection angle, θ the misorientation angle, *L* the periodic length along the GB, E_{form} the formation energy per unit length, δ the critical failure strain, and τ the intrinsic strength. "ZZ" and "AC" stand for pristine zig-zag and armchair graphene. Some values of periodic length, formation energies, and intrinsic strength from previous calculations[17,19,21,23] are also listed for comparison..

GB with higher thermodynamic stability (lower E_{form}) usually exhibits higher strength. In the flat GBs, periodic pentagon−heptagon pairs dominate the boundaries, and their ultimate strength is simply determined by the C−C bond strength as measured by the formation energy.

Among the flat boundaries explored, (3, 1)|(3, 1) and (5, 0)|(3, 3) are type IV GBs and have the highest defect concentrations, but their formation energies and intrinsic strengths are very different, *i.e.*, 3.3 eV/nm and 93 GPa for (3, 1)|(3, 1) *vs* 5.1 eV/nm and 76 GPa for (5, 0)|(3, 3). As shown in Figure 6, the (3, 1)|(3, 1) GB exhibits narrower distributions of bond length and bond angle. Namely, the atomic structure of (3, 1)|(3, 1) deviates less from the pristine graphene than (5, 0)|(3, 3); thus it is thermodynamically more stable and possesses relatively higher strength. In previous studies of carbon nanotubes[26] and nitride surfaces,[27] it was revealed that reduction of bond length can lower the binding energy and affect the mechanical properties such as strength and Young's modulus. All these results clearly indicate that the intrinsic strength of a graphene GB depends sensitively on the detailed

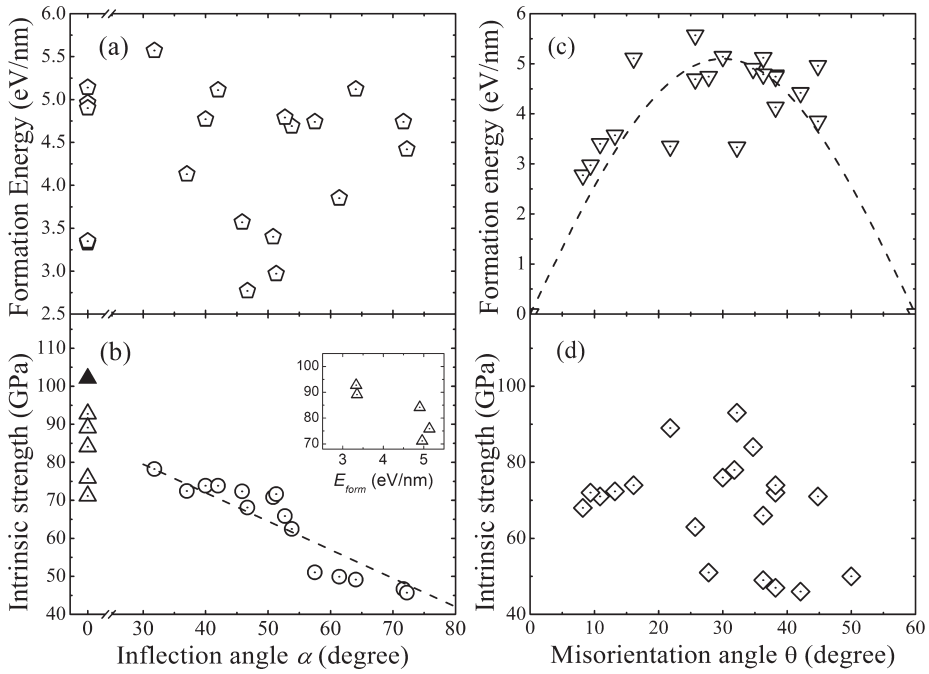

Figure 3. (a) Formation energy of a graphene GB as a function of the inflection angle α. (b) Intrinsic strength of a GB as a function of the inflection angle α: open triangles for flat GBs, open circles for inflected GBs, filled triangles for pristine graphene. The dashed line is a linear fit for those inflected GBs: τ (in GPa) = $\tau_0 - 0.75\alpha$ (τ_0 = 102 GPa). The inset graph is the intrinsic strength *versus* the formation energy for the flat GBs, showing a correlation between the two. (c) GB formation energy as a function of the misorientation angle θ. Dashed line is the sin(3θ) function. (d) Intrinsic strength *versus* misorientation angle θ, showing no clear correlation.

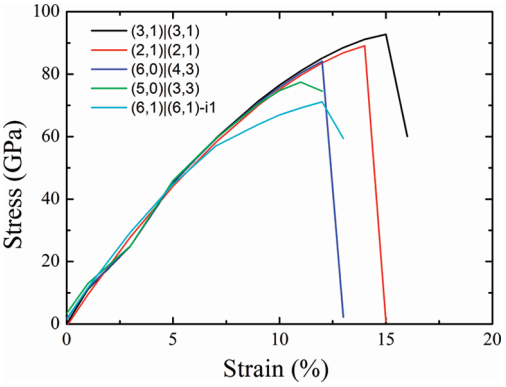

Figure 4. Stress−strain curves of flat GBs. The intrinsic strength is defined as the stress point beyond which the stress decreases with strain.

bonding environment, *e.g.*, arrangement of the pentagon/heptagon defect rings.

For the inflected GBs, especially for those with large α, pentagon and heptagon defect rings are usually distributed separately from each other along the boundary line. The isolated pentagons or heptagons induce large off-plane local distortions similar to nanocone or nanopringle[17] and, thus, significantly reduce the strength of a graphene sheet. As shown in Figure 5, the strength of buckled GBs is much lower than that of the pristine graphene and generally decreases with the inflection angle, from 78 GPa for α = 31.8° to 46 GPa for α = 72.2°. We note that of the 20 low-energy GB studies, most type I and III GBs possess larger inflection angle and weaker intrinsic strength, with the exceptions of type I GBs (2, 1)|(2, 1) and (6, 1)|(6, 1)-*i*1.

During the tensile loading of a graphene GB *via* DFT relaxations at each strain, breaking of a 7−6 bond (shared by a heptagon and hexagon) is the first sign of failure. After the 7−6 bond is broken, complete failure would occur rapidly along the boundary, and the theoretical stress would drop sharply. Mulliken population analysis[28] further revealed that there is moderate reduction of bond population (by about 5%) on this critical 7−6 bond with regard to a standard C−C bond in pristine graphene, which may weaken the C−C bond strength and facilitate the failure. The dependence of intrinsic strength on inflection angle can be related to the effective projected length of the critical 7−6 bond along the direction perpendicular to the boundary. For example, the projected length of such a 7−6 bond for the unstressed GB structure increases from 1.32 Å for (4, 1)|(3, 2)-*i*1 (α = 31.8°) to 1.47 Å for (5, 1)|(5, 1) (α = 72.2°). The elongation of the critical 7−6 bond length corresponds to larger prestrain and, thus, reduces the intrinsic strength of the graphene sheet.[23]

The boundary-induced degradation of mechanical strength can be related to previous empirical simulations of graphene sheets with a finite 1D crack modeled by slits of different lengths.[8,9] At room temperature, Zhao and Aluru found that the fracture strength decreases with crack length, from 87 GPa for pristine

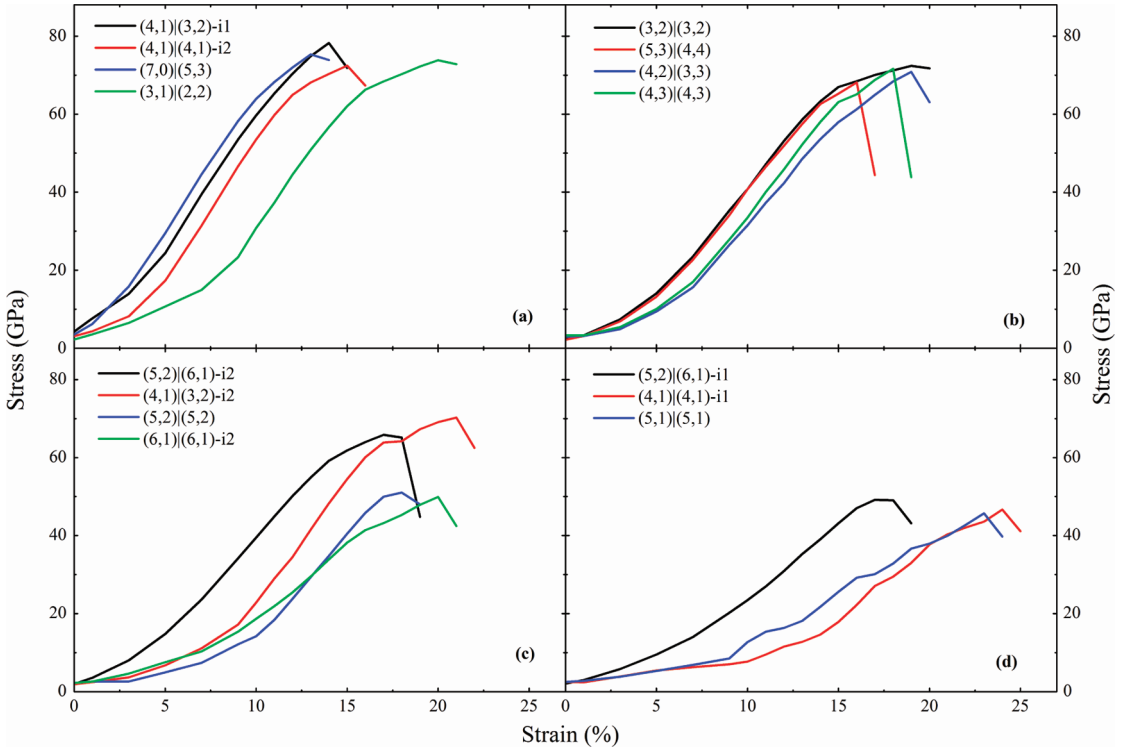

Figure 5. Stress−strain curves of inflected GBs with different ranges of inflection angle α: (a) 31.8−42°; (b) 45.85−51.3°; (c) 52.7−61.4°; (d) 64.04−72.22°.

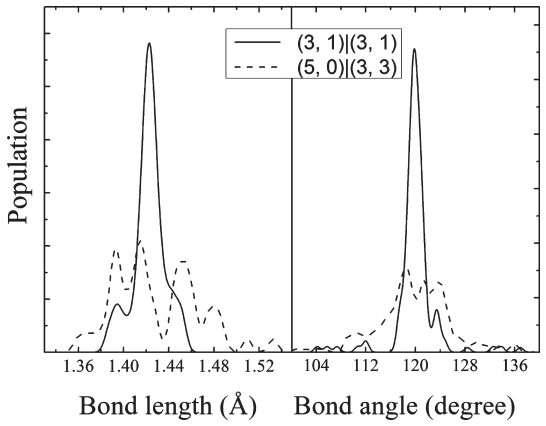

Figure 6. Distributions of the bond length (left) and the bond angle (right) for (3, 1)|(3, 1) (solid line) and (5, 0)|(3, 3) (dashed line) GBs. Even though both GBs have a high concentration of defects (see Figure 2), the narrower bond distribution in the former is correlated with its lower formation energy and higher intrinsic strength.

graphene to ~40 GPa for a graphene sheet containing a 2 nm slit.[8]

Fracture Behavior. The failure behaviors of GBs have been investigated using MD simulations. As representatives, the failure processes of (4, 1)|(3, 2)-*i*1 and (5, 0)|(3, 3) graphene GBs from empirical MD simulation are shown in Figure 7. For most GBs considered, fracture starts with the Stone−Wales (S−W) transformation of a 7−6 bond (shared by a heptagon and hexagon) on the boundary (see Figure 7). This fracture behavior resembles the "hot" mechanism for formation of S−W defects (*i.e.*, dislocation dipoles) in carbon nanotubes at high temperature.[29] As the tensile strain further increases, several fracture sites emerge simultaneously. The system eventually breaks up along the boundary at sufficiently large strain. However, for the class IV GBs with high defect density, *i.e.*, (3, 1)|(3, 1) and (5, 0)|(3, 3), the condensed arrangement of pentagons and heptagons makes the C−C bonds on the boundary stronger; thus the S−W transformation occurs in the domain region away from the boundary (Figure 7). In particular, the two parts for GB (5, 0)|(3, 3) are zigzag- and armchair-oriented graphene domains. The difference of intrinsic strengths between zigzag (102 GPa) and armchair (113 GPa) directions of graphene makes the initial fracture occur in the zigzag domain. In short, the failure behavior of a graphene GB also depends on the arrangement of defect rings and the lattice orientation of graphene in the two sides, and the fracture does not necessarily initiate from the boundary. In previous MD simulations using the NVE ensemble by Grantab *et al.*,[23] they also observed that the initial fracture sites can be either on the boundary or inside the domain. However, instead of a S−W transformation, they found that the failure started with bond breaking, which we also observe in the relaxation process. Such a difference might be attributed to the high temperature (1500 K) used in our MD simulation within the NVT ensemble, whereas the MD simulation within the NVE ensemble[23] corresponds to low-temperature situations.

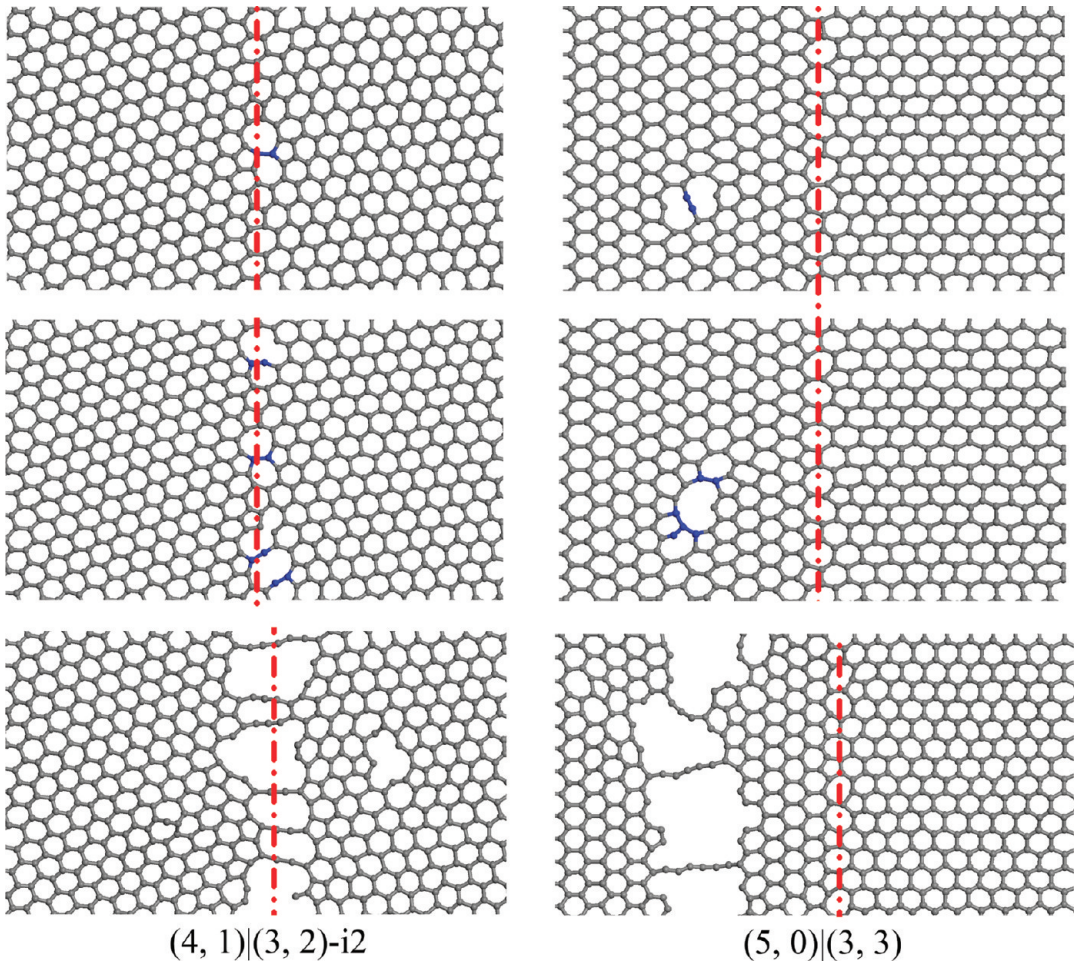

Figure 7. Failure processes of (4, 1)|(3, 2)-*i*1 (left) and (5, 0)|(3, 3) (right) graphene GBs. The atoms with Stone–Wales transformation are highlighted in blue (in the upper four graphs). The boundary lines for each GB structure are highlighted by red dashed lines as a guide for the eye. For the (4, 1)|(3, 2)-*i*1 GB, failure starts at the boundary, while failure initiates inside the domain for (5, 0)|(3, 3) GB.

CONCLUSIONS

To summarize, using the first-principles calculations and empirical molecular dynamics simulations we investigated the mechanical properties of graphene grain boundaries under tensile strains. In contrast to the $\sin(3\theta)$ dependence of the formation energy on the misorientation angle θ, there is no simple correlation between the intrinsic strength and misorientation angle. Instead, the intrinsic strength of a graphene GB depends linearly on its inflection angle α. It is found that GBs with high thermodynamic stability can be nearly as strong as pristine graphene, while the inflected GBs have a significantly reduced intrinsic strength due to buckling along the GBs. The fracture of graphene GBs was found to initiate from the Stone–Wales bond rotations at high temperatures, which can occur either on the boundary line or inside the domain.

COMPUTATIONAL METHODS

The structures and mechanical properties of graphene GBs were computed using the density functional theory (DFT) and projector-augmented wave method (PAW)[30] implemented in the VASP code.[31] The PW91 functional[32] was used to describe the exchange-correction interaction term, and the plane-wave basis was expanded up to a cutoff energy of 400 eV. An example of the simulation supercell is shown in Figure 1. A vacuum space of 1.2 nm thickness was added to the direction perpendicular to the graphene sheet. For each GB configuration, the atomic coordinates and the in-plane supercell parameters were fully relaxed.

Starting from the equilibrium geometry, a series of uniaxial tensile strains are gradually applied with 1% increment perpendicular to the boundary line, while the atomic coordinates are fully relaxed at each strain step. At each strain, the stress was computed directly for the simulation supercell using the stress theorem[33] and then rescaled by a factor of Z/d_0 to obtain the equivalent stress on the graphene sheet, where $Z = 1.2$ nm is the thickness of vacuum space and $d_0 = 0.334$ nm stands for the van der Waals thickness of the graphene sheet (which is derived from the equilibrium interlayer spacing of graphite).[34] The theoretical stress–strain curves are plotted, and the intrinsic tensile strengths were determined by the stress values at the critical failure strains, where the stress–strain curves dramatically drop. The dependence of the calculated results on the distance between

the GBs (which is half of the supercell size perpendicular to the GB direction) was investigated, with examples of result shown in Table 1. Further increasing the supersize cell leads to only minor changes of the computational results. For pristine graphene, the calculated fracture strengths are 102 GPa in the zigzag direction and 113 GPa in the armchair direction, respectively, which are comparable to previous theoretical values.[8,34−36]

The failure behaviors of these GBs were further simulated by molecular dynamics with a reactive empirical bond order potential.[37] All MD simulations were performed on a graphene monolayer of 600−1000 atoms within an NVT ensemble at 1500 K. The supercell size was about 6 × 3 × 2 nm. Within the graphene plane, tensile strains perpendicular to the boundary line were gradually applied in 1% increment until complete failure of the graphene GBs. At each strain, the system was fully relaxed for 1 ns with a MD time step of 2 fs.

Conflict of Interest: The authors declare no competing financial interest.

Acknowledgment. This work was supported by the National Natural Science Foundation of China (11134005) and the program for Changjiang Scholars and Innovative Research Team in University of China.

REFERENCES AND NOTES

1. Geim, A. K.; Novoselov, K. S. The Rise of Graphene. *Nat. Mater.* **2007**, *6*, 183–191.
2. Geim, A. K. Graphene: Status and Prospects. *Science* **2009**, *324*, 1530–1534.
3. Lee, C.; Wei, X.; Kysar, J. W.; Hone, J. Measurement of the Elastic Properties and Intrinsic Strength of Monolayer Graphene. *Science* **2008**, *321*, 385–388.
4. Hashimoto, A.; Suenaga, K.; Gloter, A.; Urita, K.; Iijima, S. Direct Evidence for Atomic Defects in Graphene Layers. *Nature* **2004**, *430*, 870–973.
5. Lusk, M. T.; Carr, L. D. Nanoengineering Defect Structures on Graphene. *Phys. Rev. Lett.* **2008**, *100*, 175503.
6. Banhart, F.; Kotakoski, J.; Krasheninnikov, A. V. Structural Defects in Graphene. *ACS Nano* **2011**, *5*, 26–41.
7. Hao, F.; Fang, D.; Xu, Z. Mechanical and Thermal Transport Properties of Graphene with Defects. *Appl. Phys. Lett.* **2011**, *99*, 041901.
8. Zhao, H.; Aluru, N. R. Temperature and Strain-rate Dependent Fracture Strength of Graphene. *J. Appl. Phys.* **2010**, *108*, 064321.
9. Khare, R.; Mielke, S. L.; Paci, J. T.; Zhang, S.; Ballarini, R.; Schatz, G. C.; Belytschko, T. Coupled Quantum Mechanical/Molecular Mechanical Modeling of the Fracture of Defective Carbon Nanotubes and Graphene Sheets. *Phys. Rev. B* **2007**, *75*, 075412.
10. Coraux, J.; N'Diaye, A. T.; Busse, C.; Michely, T. Structural Coherency of Graphene on Ir(111). *Nano Lett.* **2008**, *8*, 565–570.
11. Lahiri, J.; Lin, Y.; Bozkurt, P.; Oleynik, I. I.; Batzill, M. An Extended Defect in Graphene as a Metallic Wire. *Nat. Nanotechnol.* **2010**, *5*, 326–329.
12. Kim, K.; Lee, Z.; Regan, W.; Kisielowski, C.; Crommie, M. F.; Zettl, A. Grain Boundary Mapping in Polycrystalline Graphene. *ACS Nano* **2011**, *5*, 2142–2146.
13. Yu, Q.; Jauregui, L. A.; Wu, W.; Colby, R.; Tian, J.; Su, Z.; Cao, H.; Liu, Z.; Pandey, D.; Wei, D.; *et al.* Control and Characterization of Individual Grains and Grain Boundaries in Graphene Grown by Chemical Vapour Deposition. *Nat. Mater.* **2011**, *10*, 443–449.
14. Huang, P. Y.; Ruiz-Vargas, C. S.; van der Zande, A. M.; Whitney, W. S.; Levendorf, M. P.; Kevek, J. W.; Garg, S.; Alden1, J. S.; Hustedt, C. J.; Zhu, Y.; *et al.* Grains and Grain Boundaries in Single-Layer Graphene Atomic Patchwork Quilts. *Nature* **2011**, *469*, 389–393.
15. Cockayne, E.; Rutter, G. M.; Guisinger, N. P.; Crain, J. N.; First, P. N.; Stroscio, J. A. Grain Boundary Loops in Graphene. *Phys. Rev. B* **2011**, *83*, 195425.
16. An, J.; Voelkl, E.; Suk, J. W.; Li, X.; Magnuson, C. W.; Fu, L.; Tiemeijer, P.; Bischoff, M.; Freitag, B.; Popova, E.; *et al.* Domain (Grain) Boundaries and Evidence of "Twinlike" Structures in Chemically Vapor Deposited Grown Graphene. *ACS Nano* **2011**, *5*, 2433–2439.
17. Liu, Y.; Yakobson, B. I. Cones, Pringles, and Grain Boundary Landscapes in Graphene Topology. *Nano Lett.* **2010**, *10*, 2178–2183.
18. Yazyev, O. V.; Louie, S. G. Electronic Transport in Polycrystalline Graphene. *Nat. Mater.* **2010**, *9*, 806–809.
19. Yazyev, O. V.; Louie, S. G. Topological Defects in Graphene: Dislocations and Grain Boundaries. *Phys. Rev. B* **2010**, *81*, 195420.
20. Malola, S.; Hakkinen, H.; Koskinen, P. Structural, Chemical, and Dynamical Trends in Graphene Grain Boundaries. *Phys. Rev. B* **2010**, *81*, 165447.
21. Liu, T. H.; Gajewski, G.; Pao, C. W.; Chang, C. C. Structure, Energy, and Structural Transformations of Graphene Grain Boundaries from Atomistic Simulations. *Carbon* **2011**, *49*, 2306–2317.
22. Yakobson, B. I.; Ding, F. Observational Geology of Graphene, at the Nanoscale. *ACS Nano* **2011**, *5*, 1569–1574.
23. Grantab, R.; Shenoy, V. B.; Ruoff, R. S. Anomalous Strength Characteristics of Tilt Grain Boundaries in Graphene. *Science* **2010**, *330*, 946–948.
24. Xu, Z. P.; Buehler, M. J. Geometry Controls Conformation of Graphene Sheets: Membranes, Ribbons and Scrolls. *ACS Nano* **2010**, *4*, 3869–876.
25. Koskinen, P.; Malola, S.; Hakkinen, H. Self-Passivating Edge Reconstructions of Graphene. *Phys. Rev. Lett.* **2008**, *101*, 115502.
26. Sun, C. Q.; Bai, H. L.; Tay, B. K.; Li, S.; Jiang, E. Y. Dimension, Strength, and Chemical and Thermal Stability of a Single C-C Bond in Carbon Nanotubes. *J. Phys. Chem. B* **2003**, *107*, 7544–7546.
27. Sun, C. Q.; Tay, B. K.; Lau, S. P.; Sun, X. W.; Zeng, X. T.; Li, S.; Bai, H. L.; Liu, H.; Liu, Z. H.; Jiang, E. Y. Bond Contraction and Lone Pair Interaction at Nitride Surfaces. *J. Appl. Phys.* **2001**, *90*, 2615–2617.
28. Segall, M. D.; Shah, R.; Pickard, C. J.; Payne, M. C. Population Analysis of Plane-Wave Electronic Structure Calculations of Bulk Materials. *Phys. Rev. B* **1996**, *54*, 16317–16320.
29. Dumitrica, T.; Hua, M.; Yakobson, B. I. Symmetry-, Time-, and Temperature-Dependent Strength of Carbon Nanotubes. *PNAS* **2006**, *103*, 6105–6109.
30. Kresse, G.; Joubert, D. From Ultrasoft Pseudopotentials to the Projector Augmented-Wave Method. *Phys. Rev. B* **1999**, *59*, 1758.
31. Kresse, G.; Furthmuller, J. Efficient Iterative Schemes for ab Initio Total-Energy Calculations Using a Plane-Wave Basis Set. *Phys. Rev. B* **1996**, *54*, 11169; Efficiency of ab-initio Total Energy Calculations for Metals and Semiconductors Using a Plane-wave Basis Set. *Comput. Mater. Sci.* **1996**, *6*, 15–50.
32. Perdew, J. P.; Wang, Y. Accurate and Simple Analytic Representation of the Electron-Gas Correlation Energy. *Phys. Rev. B* **1992**, *45*, 13244.
33. Nielsen, O. H.; Martin, R. M. First-Principles Calculation of Stress. *Phys. Rev. Lett.* **1983**, *50*, 697; Quantum-Mechanical Theory of Stress and Force. *Phys. Rev. B* **1985**, *32*, 3780.
34. Liu, F.; Ming, P.; Li, J. Ab initio Calculation of Ideal Strength and Phonon Instability of Graphene under Tension. *Phys. Rev. B* **2007**, *76*, 064120.
35. Xiao, J. R.; Staniszewski, J.; Gillespie, J. W., Jr. Fracture and Progressive Failure of Defective Graphene Sheets and Carbon Nanotubes. *Compos. Struct.* **2009**, *88*, 602–609; Tensile Behaviors of Graphene Sheets and Carbon Nanotubes with Multiple Stone−Wales Defects. *Mater. Sci. Eng. A* **2010**, *527*, 715–723.
36. Marianetti, C. A.; Yevick, H. G. Failure Mechanisms of Graphene under Tension. *Phys. Rev. Lett.* **2010**, *105*, 245502.
37. Brenner, D. W.; Shenderova, O. A.; Harrison, J. A.; Stuart, S. J.; Ni, B.; Sinnott, S. B. A Second-Generation Reactive Empirical Bond Order (REBO) Potential Energy Expression for Hydrocarbons. *J. Phys.: Condens. Matter* **2002**, *14*, 783–802.